



## Electronic structure of Cr–Al alloy: Theory and experiment

Alpa Dashora, B.L. Ahuja\*

Department of Physics, University College of Science, M.L. Sukhadia University, Udaipur, 313001 Rajasthan, India

### ARTICLE INFO

#### Article history:

Received 5 January 2010  
Received in revised form 5 April 2010  
Accepted 7 April 2010

#### PACS:

13.60.Fz  
72.15.–v  
78.70.Ck

#### Keywords:

X-ray scattering  
Compton profile  
Electronic structure of alloy

### ABSTRACT

First ever Compton spectroscopy study on  $\text{Cr}_{0.8}\text{Al}_{0.2}$  alloy to examine the charge transfer and electron momentum densities using in-house  $^{241}\text{Am}$   $\gamma$ -ray spectrometer is presented. The experimental data on the alloy are compared with present spin polarized relativistic Korringa–Kohn–Rostoker (SPR–KKR) calculations. The experimental Compton data on the alloy and its constituents, and SPR–KKR electronic structure calculations predict charge transfer from  $\text{Cr} \rightarrow \text{Al}$  on alloying. Present computations of valence band X-ray photoemission spectra are found to be in good agreement with the available experimental data.

© 2010 Elsevier B.V. All rights reserved.

### 1. Introduction

AlM alloys, where M stands for a 3d transition metal, have several technological applications [see, for example, Refs. [1,2]]. Among these alloys, Cr–Al system is mainly known to be a primary material for structural components of an aircraft. Earlier studies on Cr–Al alloys mainly include magnetic and electrical transport properties [3], transmission electron microscopy and X-ray diffraction measurements, etc. [4,5], photoemission studies [6] and cluster calculations [7], etc.

Determination of charge transfer is a fundamental problem in condensed matter physics. It is frustratingly difficult to measure the charge transfer in case of disordered alloys like Cr–Al system. Therefore, there is need for an accurate and reliable method to determine the electronic structure of systems which are without a perfect translational symmetry. The restriction to surface (in angle resolved photoemission spectroscopy), thin films (in e, 2e method), low defects (in angular correlation of annihilation method) and low temperature (in de Hass–van Alphen technique) does limit the applications of different spectroscopic techniques. On the other hand, applicability of Compton spectroscopy is not limited to systems with low defects or impurities. Moreover, this methodology is not complicated like photoemission or electron scattering technique. Now we give a brief account of the Compton spectroscopy.

The Compton scattering technique is uniquely employed to probe the electronic structure of materials. The Compton profile can be deduced by measuring the double differential scattering cross-section [8,9]. Mathematically,

$$\frac{d^2\sigma}{d\Omega d\omega_2} \propto J(p_z) = \int \int n(\vec{p}) dp_x dp_y \quad (1)$$

where  $p_z$  is the component of electron momentum along the scattering vector and  $n(\vec{p})$  is the electron momentum density. The relationship holds within the impulse approximation which requires that the energy transferred to electrons is larger than their binding energies. The  $n(\vec{p})$  is connected to the real space wave function through the Fourier transformation

$$n(\vec{p}) \propto \sum_j^{\text{occ}} \int |\psi(\vec{r}_j) e^{i\vec{p}\cdot\vec{r}}|^2 d\vec{r} \quad (2)$$

The summation index in Eq. (2) is over all the occupied states. Therefore, the Compton scattering is sensitive to probe the behaviour of valence electrons. It is known that different valence band electrons have their characteristic Compton profiles, which are reflected in overall shape of Compton profiles of materials.

To our knowledge, till date, theoretical or experimental momentum densities of this system are not available in literature. In this paper, we present Compton profiles and electronic properties of disordered  $\text{Cr}_{0.8}\text{Al}_{0.2}$  alloy.

The purpose of present work is (a) to measure the momentum densities of Cr–Al system along with the constituent elements

\* Corresponding author. Tel.: +91 94 143 17048.  
E-mail address: [blahuja@yahoo.com](mailto:blahuja@yahoo.com) (B.L. Ahuja).

and compare the data with electronic structure calculations, (b) to established the *in-house*  $\gamma$ -ray Compton scattering technique as a probe to find out charge transfer in disordered alloys where other rival techniques may have certain limitations and (c) to compute the X-ray photoemission data, etc.

## 2. Methodology

### 2.1. Experiment

To measure the isotropic Compton profiles of  $\text{Cr}_{0.8}\text{Al}_{0.2}$  and the constituent elements, we have employed our  $^{241}\text{Am}$  Compton spectrometer [10]. The polycrystalline samples in form of pellet (thickness 0.3 cm and dia. 2.0 cm) for Cr and Cr–Al alloy, and a thin sheet (thickness 0.2 cm and dia. 2.0 cm) of Al have been used for the present measurements. The individual samples were placed vertically in the scattering chamber and radiations scattered at an angle of  $165 \pm 0.5^\circ$  have been analysed with a high purity Ge crystal. The overall momentum resolution of the spectrometer was 0.55 a.u. Gaussian full width at half-maximum (FWHM). The measurements have been taken for 86.9, 70.5 and 35.8 h for Cr, Cr–Al alloy and Al, respectively.

The raw Compton profiles were corrected for several systematic corrections like, background subtraction, instrumental resolution (limited to stripping off the low energy tail), sample absorption, Compton cross-section and multiple scattering, etc. [8,9]. Finally, the experimental profiles were normalised to the area of corresponding free-atom Compton profile in the range 0–7 a.u. [11].

### 2.2. Theory

To calculate the density of states (DOS), valence band X-ray photoemission spectra (XPS) and Compton profiles, we have used the spin polarized relativistic Korringa–Kohn–Rostoker (SPR-KKR) method [12,13]. Instead of the electronic wave functions and eigen values, the KKR aims to calculate the single-particle Green's function. Using Green's function, one can calculate all single-particle expectation values of a crystal like particle density or other quantities important in material science, such as DOS and magnetic moment. In order to determine the Green's function of the system at a fixed energy,  $t$ -matrix is determined which describes the scattering on each individual non-overlapping atomic, spatially bounded potentials [12,13]. The atomic  $t$ -matrices and the crystal structure parameter  $G$ , can be combined to construct the scattering path operator  $\tau$ . The  $\tau$  describes all possible scattering events for a single electron on its way between two individual scattering centers and therefore it is a central quantity to construct the Green's function for the entire system.

In the present calculations, we have employed coherent potential approximation (CPA), which is a mean field approximation where the homogeneity of disorder restores the translational symmetry using the averaged quantity. The SPR-KKR-CPA approach turns out to be a reliable tool to study the electronic structure of binary disordered alloys. Within the CPA prescription, the configurationally averaged properties of a disordered alloy are derived from a hypothetical ordered CPA-medium that may be described by the following condition

$$x_A \tau^{\text{nn,A}} + x_B \tau^{\text{nn,B}} = \tau^{\text{nn}} \quad (3)$$

where  $\tau^{\text{nn}}$  is the scattering path operator corresponding to CPA-medium.  $\tau^{\text{nn,A}}$  and  $\tau^{\text{nn,B}}$  describe the total scattering due to a single atom of type A and B respectively, which are embedded in the effective coherent potential medium [12–14]. The sites A and B are occupied by the constituent atoms A and B with relative probability  $x_A (=x)$  and  $x_B (=1-x)$ , respectively.

To compute the XPS data employing SPR-KKR-CPA approach, an expression for intensity  $I(E, \vec{k}, m_s; \omega, \vec{q}, \lambda)$  of the photoelectron current [12–14] observed in valence band photoemission can be deduced by starting from Fermi's Golden rule as:

$$I(E, \vec{k}, m_s; \omega, \vec{q}, \lambda) \propto \sum_{\text{initial states } i} \left| d^3 r \phi_{\vec{k}, m_s}^{\text{final}}(\vec{r}, E) X_{\vec{q}\lambda}(\vec{r}) \phi_i(\vec{r}, E_i) \right|^2 \times \delta(E - \omega - E_i) \quad (4)$$

The operator  $X_{\vec{q}\lambda}$  describes the interaction of the electrons and the radiation field with the vector potential  $\vec{A}_{\vec{q}\lambda}$  representing the radiations with energy  $\omega$ , wave vector  $\vec{q}$  and polarization  $\lambda$ . The summation extends over all possible initial states  $\phi_i$  allowed by energy conservation and selection rules which are primarily detected by the operator  $X_{\vec{q}\lambda}$ . In the Eq. (4), the photoelectrons have energy  $E$ , wave vector  $\vec{k}$  and spin polarization  $m_s$ . The  $\phi_{\vec{k}, m_s}^{\text{final}}$  is the corresponding final state.

In the present computations, the parameterisation for the exchange–correlation potential of Vosko, Wilk and Nusair (VWN) [15] was used. For self-consistent-field (SCF) calculations, the BROYDEN2 scheme (an iterative quasi-Newton method to solve the systems of non-linear equations) was considered. The number of  $\mathbf{k}$  points for SCF cycles were taken to be 10,648, which resulted 834  $\mathbf{k}$  points in the irreducible 1/48th part of the Brillouin zone. For a better convergence, the SCF mixing parameter was set to 0.20. For the alloy and its constituents, the isotropic valence band Compton profiles were computed using spherical average of directional profiles derived along [1 0 0], [1 1 0] and [1 1 1] directions. To evaluate the absolute profiles, the profiles due to core electrons were taken from the free-atom Compton profiles tables [11] as these electrons are described reasonably well by free-atom wave functions [8,9]. The isotropic theoretical Compton profiles were convoluted with a FWHM of 0.55 a.u., to match with the experimental resolution.

## 3. Results and discussion

### 3.1. DOS

The total and partial DOS for alloy and individual constituent elements using SPR-KKR are shown in Fig. 1(a)–(c). In Fig. 1(a), the total DOS of Al almost shows homogeneous DOS all over the region of energy. It is understandable because Al possesses an almost spherical Fermi surface. In the energy range  $-2$  to  $-4$  eV, the Al 2p states are found to be dominating. DOS curves for Cr, as shown in Fig. 1(b), depict that the total DOS are dominated by Cr 3d states; whereas Cr 4s states appear mainly below  $-2$  eV. In case of alloy [Fig. 1(c)], it is seen that the major structures in the DOS are broadened in comparison to its constituent Cr. The change in amplitude and broadening in DOS after the formation of alloy show the failure of the superposition concept. Therefore, change in DOS on the alloying may be attributed to charge transfer within the constituents.

### 3.2. Compton profiles and determination of charge transfer

Fig. 2(a) shows a comparison of the absolute experimental and convoluted theoretical (SPR-KKR) profiles. In the high-momentum region (5.0 a.u.), all the individual theoretical profiles are in good agreement with their respective experimental data. This is only to be expected because in the high-momentum range the contribution is mainly from the core electrons and the wave function of these electrons are free-atom like. To illustrate the difference in the low momentum side, we have plotted the difference between absolute convoluted theoretical profiles and the related experiment in Fig. 1(b). It is seen that in the vicinity of  $J(0)$ , the Al experimen-

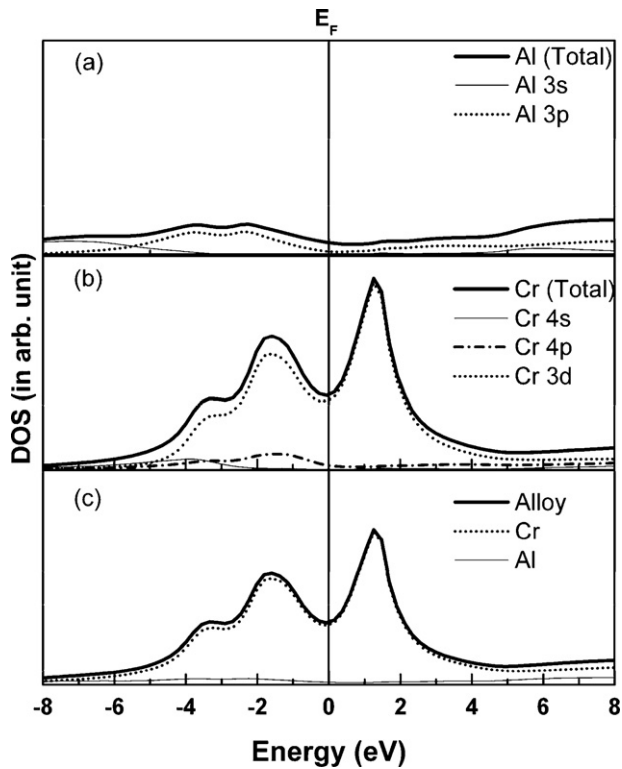


Fig. 1. Partial and total density of states computed using SPR-KKR calculations for (a) Al (b) Cr and (c)  $\text{Cr}_{0.8}\text{Al}_{0.2}$  along with constituents within the alloy.

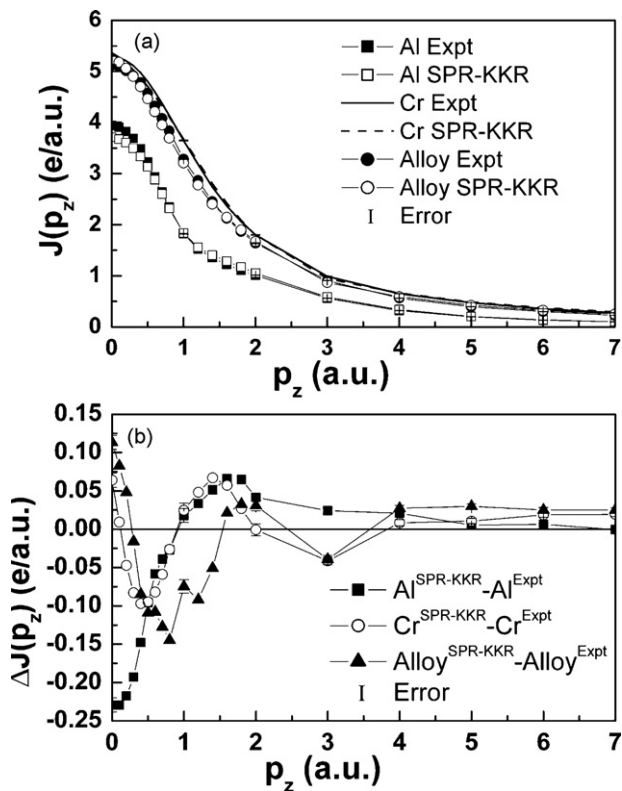


Fig. 2. (a) Absolute experimental and convoluted theoretical Compton profiles and (b) difference between absolute theoretical and experimental Compton profiles of Al, Cr and CrAl alloy. All the theoretical profiles are convoluted with a Gaussian FWHM of 0.55 a.u.

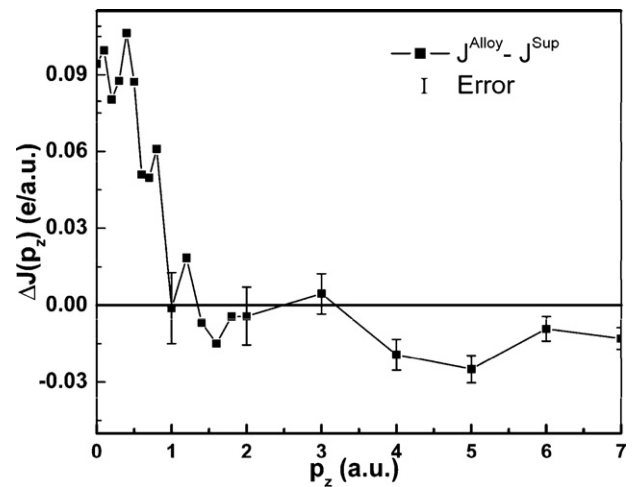


Fig. 3. Difference between Compton profile of alloy,  $J^{\text{Alloy}}$ , and superposition profile,  $J^{\text{sup}}$ , deduced from the individual experimental data ( $0.8J_{\text{Expt}}^{\text{Cr}} + 0.2J_{\text{Expt}}^{\text{Al}}$ ). Statistical errors are shown at few points.

tal profile is found to be lower than the corresponding theory. A reasonable agreement between experimental alloy profile and SPR-KKR calculations shows the applicability of SPR-KKR prescription for disordered alloys. A few subtle differences between the electronic structure of the alloys and its constituents may emerge from their band dispersions and hence the DOS.

The difference in experimental Compton profile of alloy and superposition profile of its constituents, which gives information about the change in the outer electron states when the alloy is formed, is given in Fig. 3. The trend of the difference profile depicts that the alloy profile is 'broader' than the superposition profile, which is resulted from the sum of profiles of constituents. In terms of charge transfer, it means that charge transfer may be towards high-momentum orbitals like  $s \rightarrow p$ .

Our previous experience [16,17] has shown that the Compton profiles of alloys can be analysed in terms of individual contributions of the constituents. The key is that the momentum distribution is built from the superposition of the contribution from different electrons of the constituents. In comparison to Al, the valence band Compton profile of Cr extends to higher momentum. A quantitative comparison of momentum densities shows that the valence electron Compton profiles of Cr and Al have half widths which differ by more than 40%. Therefore, the valence profile of the alloy can be synthesized when the valence band profiles of the constituents are fitted over the whole momentum range. We have used the following least square relation

$$E = \sum_{p_z=0}^{7.0 \text{ a.u.}} [J_{\text{Alloy}}^{\text{Val.Expt}}(p_z) - mJ_{\text{Cr}}^{\text{Val.Expt}}(p_z) - nJ_{\text{Al}}^{\text{Val.Expt}}(p_z)]^2 \quad (5)$$

in fitting of individual experimental valence profiles of Cr and Al to the alloy valence experimental Compton line. The sum extends over the available experimental data points. The weight coefficients  $m$  and  $n$  are computed for the best fit to the alloy valence band Compton profile. To compute the valence band experimental Compton profile of Cr–Al alloy and its constituents, we have subtracted the respective convoluted free-atom core profile [11] from the experimental profiles. In Fig. 4(a), the experimental valence Compton profile of alloy, its decomposition into the Cr and Al valence profiles and the best fitted profile in the range 0–7 a.u. are plotted. The number of electrons on the individual sites (Table 1) is simply the area under the component curves. Within free-atom environment, valence electrons of Al and Cr in the fractional composition of the alloy are expected to be 0.60 and 4.80 $e^-$ , respectively. From

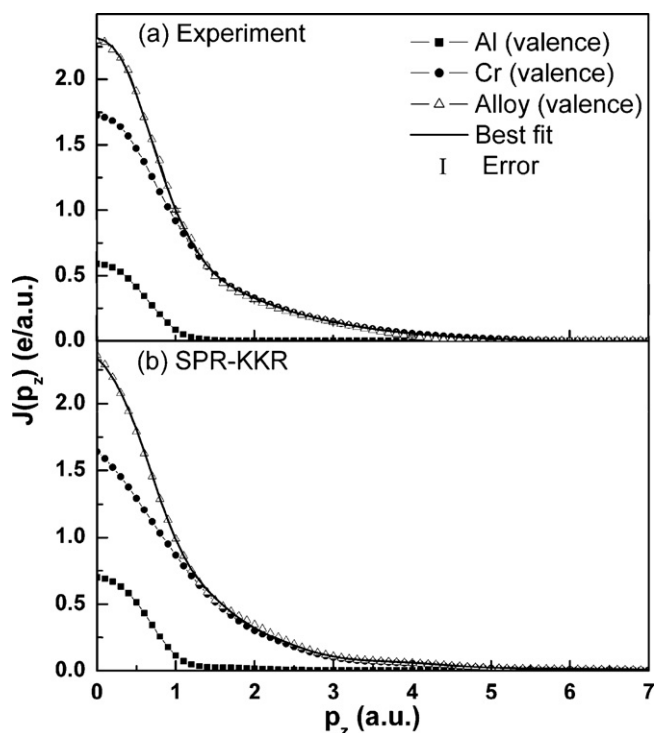


**Fig. 4.** Decomposition of (a) experimental and (b) theoretical valence Compton profiles of  $\text{Cr}_{0.8}\text{Al}_{0.2}$  alloy into the valence band momentum density of Al and Cr. The area under the individual profile is equal to the number of valence band electrons.

Fig. 4(a), it is seen that after alloy formation, occupancies of Al and Cr comes out to be  $0.80$  and  $4.64e^-$ , respectively. Therefore, a charge transfer from Cr to Al is predicted which is given in Table 1 along with X-ray photoemission spectroscopy (XPS) data of Jablonska et al. [6]. It is interesting to note a small difference between the charge transfer deduced from Compton (bulk study) and the XPS (surface study) measurements.

To ensure the direction of charge transfer qualitatively, as done in experimental work, we have also decomposed the SPR-KKR based profile into the individual SPR-KKR based valence profile of Al and Cr. The best fit is shown in Fig. 4(b). Following the similar methodology, a theoretical charge transfer of about  $0.4e^-$  from Cr  $\rightarrow$  Al is observed. Therefore, the present work which employs  $^{241}\text{Am}$  Compton spectrometer (momentum resolution  $0.55$  a.u.) confirms that *in-house* low-intensity  $\gamma$ -ray Compton spectrometers may be successfully employed for a reasonable estimation of charge transfer in disordered alloys, where the other spectroscopic techniques may fail.

**Table 1**

The charge transfer determination by the analysis of valence band experimental momentum densities. XPS data is also shown for a comparison.

Definition	Present experiment	
	Before fitting	After fitting
(a) Present experiment		
Al (valence band)	$0.60e^-$	$0.80e^-$
Cr (valence band)	$4.80e^-$	$4.64e^-$
Alloy (valence band)	$5.40e^-$	$5.44e^-$
Predicted charge transfer <sup>a</sup> (Cr $\rightarrow$ Al)	$0.18 \pm 0.04e^-$ (Cr $\rightarrow$ Al)	
(b) XPS data [6]	$0.20e^-$ (Cr $\rightarrow$ Al)	

<sup>a</sup> Average value of  $0.20$  ( $0.80e^-$  to  $0.60e^-$ ) and  $0.16$  ( $4.80e^-$  to  $4.64e^-$ ).

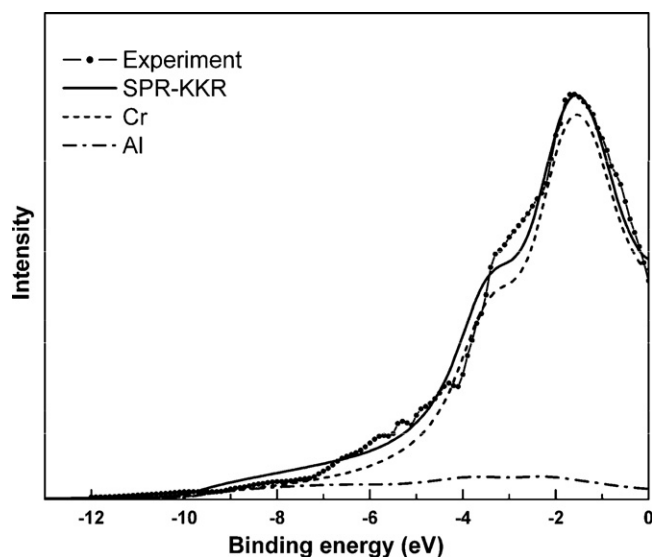


**Fig. 5.** The theoretical XPS data calculated using SPR-KKR-CPA along with the experimental data [6] for CrAl alloy. The individual data for Cr and Al represent the components in the alloy environment.

### 3.3. XPS

Our SPR-KKR based XPS spectra for the CrAl alloy along with its constituents and available experimental data [6] are shown in Fig. 5. The experimental data [6] were obtained using unpolarized Al  $K\alpha$  radiation with an energy  $\hbar\omega = 1486.6$  eV. To compare our theoretical XPS data with the available experiment, we have convoluted the theory with the experimental resolution of XPS set-up. The theoretical data have been arbitrarily shifted in energy so as to obtain the coincidence with the intense peak (at about  $-2$  eV) of experimental data. A remarkable agreement between the theoretical (KKR) and experimental XPS in terms of intensity and broadening near  $-2$  eV is observed. A similarity between overall shape of shoulders in the theoretical XPS data for the alloy and Cr near  $-2$  eV is also found. In the experimental data the shoulder is smeared out which may be, partially, due to the limited resolution of the experiment.

### 4. Conclusions

The experimental and theoretical (SPR-KKR) Compton profiles of  $\text{Cr}_{0.8}\text{Al}_{0.2}$ , Cr and Al are presented. In this trend-setting paper, Compton profiles using in-house  $\gamma$ -ray spectrometer and SPR-KKR model are analysed mainly in terms of momentum densities and quantitative charge transfer on the formation of alloys. The methodology suggested in the present paper has a great potential in determination of even small charge transfer using low-intensity  $^{241}\text{Am}$  Compton spectrometers. It is seen that the SPR-KKR calculations are in reasonable agreement with the available XPS measurements.

### References

- [1] P.P. Singh, Phys. Rev. B 43 (1991) 3975–3985.
- [2] D. Guenzburger, D.E. Ellis, Phys. Rev. B 45 (1992) 285–294.
- [3] S. Araj, N.L. Reeves, E.E. Anderson, J. Appl. Phys. 42 (1971) 1691–1692.
- [4] P.A. Bancel, P.A. Heiney, Phys. Rev. B 33 (1986) 7917–7922.
- [5] V.T. Swamy, S. Ranganathan, K. Chattopadhyay, J. Mater. Res. 4 (1989) 539–551.
- [6] K.L. Jablonska, E. Minni, J. Pelka, E. Suoninen, J. Auleytner, Phys. Stat. Sol. B 123 (1984) 627–634.
- [7] D. Bagayoko, P.M. Lam, N. Brener, J. Callaway, Phys. Rev. B 54 (1996) 12184–12193.
- [8] M.J. Cooper, Rep. Prog. Phys. 48 (1985) 415–481.
- [9] M.J. Cooper, P.E. Mijnarends, N. Shiotani, N. Sakai, A. Bansil, X-ray Compton Scattering, Oxford Univ. Press, Oxford, 2004.

- [10] B.L. Ahuja, V. Sharma, A. Rathor, A.R. Jani, B.K. Sharma, *Nucl. Instrum. Methods B* 262 (2007) 391–398.
- [11] F. Biggs, L.B. Mandelsohn, J.B. Mann, *Atom. Data Nucl. Data Tables* 16 (1975) 201–308.
- [12] The Munich SPR-KKR packages, version 3.6, H. Ebert et al., <http://olymp.cup.uni.muenchen.de/ak/ebert/SPRKKR>.
- [13] H. Ebert, in: H. Dressé (Ed.), *Electronic Structure and Physical Properties of Solids*, vol. 535, Springer, Berlin, 2000, p. 191.
- [14] D. Benea, S. Mankovsky, H. Ebert, *Phys. Rev. B* 73 (2006), (094411-1-094411-6).
- [15] S.H. Vosko, L. Wilk, M. Nusair, *Can. J. Phys.* 58 (1980) 1200–1211.
- [16] B.L. Ahuja, B.K. Sharma, S. Mathur, N.L. Heda, M. Itou, A. Andrejczuk, Y. Sakurai, A. Chakrabarti, S. Banik, A.M. Awasthi, S.R. Barman, *Phys. Rev.* 75B (2007) (134403-1-134403-9).
- [17] B.L. Ahuja, G. Ahmed, S. Banik, M. Itou, Y. Sakurai, S.R. Barman, *Phys. Rev.* 79B (2009) (214403-1-214403-6).